

Polymer Electronics: To Be or Not to Be?

Paul W. M. Blom

The realization that polymers can be used as active material in opto-electronic applications initiated substantial effort in the scientific community to explore new materials. Polymers can be made strong, flexible, lightweight, and can be mass produced. Furthermore, polymers can be processed at low temperatures, typically below 150 °C, creating the opportunity to use a range of plastic substrates instead of glass. Many polymers are soluble in organic solvents, making it possible to create electronically active “inks” that allow for solution-processed electronic components as light-emitting diodes and transistors. Examples of innovative new products based on semiconducting polymers are inkjet-printed displays, non-contact radio frequency identification tags, and sensors. However, the realization of polymeric displays is hindered by the relatively low efficiency of polymer-based light-emitting diodes. Major problems are the inability to realize multi-layers from solution, insufficient harvesting of triplet excitons and the presence of defects. Printed circuits of organic transistors are still hampered by stability issues and relatively low charge carrier mobility of the organic semiconductors. More recently, organic electrochemical transistors have been employed as biosensors. Herein, the fundamentals and recent progress of polymer-based light-emitting devices and transistors are being discussed.


(inkjet) printed displays^[3] and integrated circuits for application in radio-frequency identification tags.^[4] A few years later, semiconducting polymers became attractive as active layer in organic solar cells.^[5] More recently, polymeric semiconductors have also been applied in sensing devices.^[6] However, to date, only optoelectronic devices based on small molecules are commercially available.^[7] These materials are usually vacuum-deposited, enabling the deposition of several organic layers on top of each other.^[8] Commercial OLED displays use complex multilayer device architectures to achieve balanced charge transport and confine the charge carriers in the emission layer.^[9] To further enhance efficiency new materials such as phosphorescent^[10,11] and thermally-activated delayed fluorescence (TADF) emitters^[12,13] have been developed to harvest triplet excitons. Furthermore, new device architectures such as p-i-n type based on doped charge injection and transport layers are being used to reduce the operating voltage of OLEDs.^[14] Realizing such a complex

multilayer with solution-processed semiconductors as conjugated polymers is very difficult. The solvent used to deposit a subsequent layer may redissolve the layer underneath. The inability to realize multilayers and to efficiently harvest triplet excitons strongly limited the efficiency of early generation PLEDs. However, despite their low device performances the attractive properties of conjugated polymers as flexibility, low-weight, low cost of manufacturing and biocompatibility remain. To exploit these beneficial properties in future optoelectronic devices further understanding of their fundamental properties and limits to the device performances are required. In the following sections the fundamentals and recent progress of polymer based light-emitting devices and transistors are being discussed.

1. Introduction

Shirakawa, MacDiarmid, and Heeger reported in 1977 a dramatic increase in electrical conductivity of the semiconducting polymer polyacetylene by doping it with halogen ions or with arsenic pentafluoride (AsF₅).^[1] For their discovery and development of conductive polymers the scientists were honored with the Nobel Prize for Chemistry in 2000. After this breakthrough, conjugated polymers gained considerable attraction for application in optoelectronic devices due to their mechanical and optical properties and potential low-cost manufacturing using printing techniques. Especially the invention of the polymer light-emitting diode (PLED) boosted the field of polymer-based devices.^[2] Initially, the focus was on the realization of polymer-based

Prof. P. W. M. Blom
Max Planck Institute for Polymer Research
Ackermannweg 10, Mainz 55128, Germany
E-mail: blom@mpip-mainz.mpg.de

 The ORCID identification number(s) for the author(s) of this article can be found under <https://doi.org/10.1002/admt.202000144>.

© 2020 The Authors. Published by WILEY-VCH Verlag GmbH & Co. KGaA, Weinheim. This is an open access article under the terms of the Creative Commons Attribution License, which permits use, distribution and reproduction in any medium, provided the original work is properly cited.

DOI: 10.1002/admt.202000144

2. PLEDs

PLEDs in its simplest form consist of a vertical stack where the emissive layer is sandwiched between two electrodes. The operation of a PLED relies on three features, which are charge injection, charge transport, and recombination, as schematically shown in **Figure 1**. First, holes and electrons are injected from the electrodes into the organic semiconductors by applying a positive voltage on the anode and a negative voltage on the cathode, respectively.

Due to the applied electric field electrons and holes will drift to the opposite electrode. When the distance between a hole and

an electron is close enough, they will be attracted by Coulomb interaction to form an exciton, a bound excited state between a hole and electron. Subsequently, the exciton decays radiatively to its ground state by emission of a photon. To evaluate the performance of PLEDs the external quantum efficiency (EQE) is used, defined as the ratio between the number of emitted photons in the direction of the viewer and the amount of injected carriers. Early generations of PLEDs were based on fluorescent emitters, meaning that only 25% of the formed excitons, the singlet excitons, are contributing to the light-output of the PLED. The remaining 75%, the triplet excitons, decay non-radiatively to the ground state, since this is an optically forbidden transition. Furthermore, since the refractive index of organic semiconductors (≈ 1.7 – 1.8) is higher than the one of glass (1.5%) and air (1.0) typically around 80%, of the 25% radiative singlet excitons are being trapped in the PLED structure due to internal reflections, the so-called outcoupling loss. Combining the losses due to triplet exciton formation (75%) and optical outcoupling (80%), the maximum EQE of a PLED would be limited to only 5%, which is far too low for applications. In many cases, reported EQEs of PLEDs were even lower, in the range of 1–2%. To understand the origin of these loss processes we first discuss the charge transport and recombination process in conjugated polymers.

2.1. Charge Transport and Recombination in Conjugated Polymers

A first requirement for an efficient PLED is the realization of efficient charge injection; charges injected by the electrodes must overcome or tunnel through a barrier between the HOMO/LUMO of the emissive polymer and the electrode work function. Efficient charge injection can therefore be realized

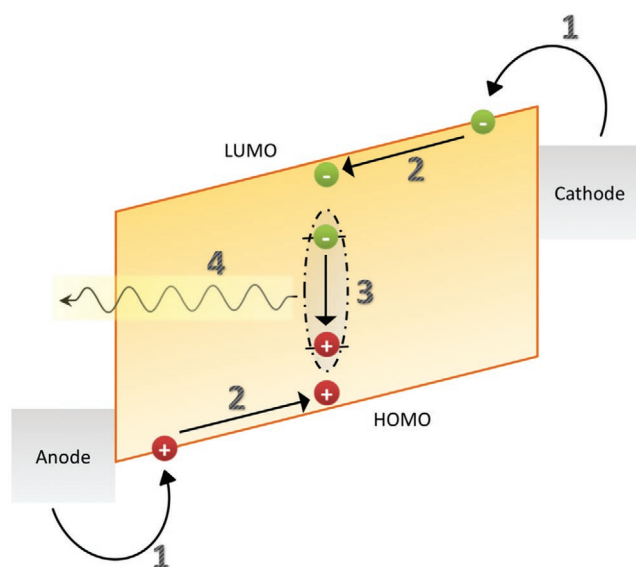


Figure 1. Schematic illustration of the operation of a PLED. 1) Charge injection from the electrodes occurs upon application of a voltage. 2) Holes and electrons are transported toward the cathode and the anode, respectively, due to the applied electric field. 3) When a hole and an electron meet, they recombine to form an exciton, which decays 4) with subsequent emission of light.



Paul W. M. Blom received his Ph.D. degree in 1992 from the Technical University Eindhoven on picosecond charge carrier dynamics in GaAs. At Philips Research Laboratories he was engaged in the electro-optical properties of polymer light-emitting diodes. From 2000 he held a professorship at the University of Groningen in

the field of electrical and optical properties of organic semiconducting devices. In September 2008 he became a scientific director of the Holst Centre in Eindhoven, where the focus is on foil-based electronics, followed in 2012 by an appointment as a director at the MPI for polymer research in the field of molecular electronics.

when the work function of the anode and cathode match the HOMO and LUMO of the active layer, respectively.^[15,16] When the contacts are ohmic, the device current is limited by bulk transport. For PLEDs based on derivatives of poly(p-phenylene vinylene) (PPV) it was shown that the hole transport is governed by a (bulk) space-charge limited current (SCLC).^[17] In this type of transport, the amount of injected charges into the device per unit time is limited by the electrostatic field as a result of space-charge build-up. The SCLC as derived by Mott and Gurney is given by^[18]

$$J_{\text{SCL}} = \frac{9}{8} \epsilon_0 \epsilon_r \mu \frac{V^2}{L^3} \quad (1)$$

with V the applied voltage, L the active layer thickness, ϵ_0 ϵ_r the permittivity and μ the charge carrier mobility. An important aspect in the transport of organic semiconductors is the presence of disorder. Typically, conjugated polymer chains contain kinks and defects that lead to a break in conjugation. Therefore, polymer chains can be considered as consisting of segments with different conjugation length and consequently different energy states. This energy distribution leads to spreading in site energies, so-called energetic disorder,^[19] as schematically shown in Figure 2.

It has been shown that the trap-free hole transport at room temperature in most of the conjugated polymers can be described by the SCLC model but only at low voltages.^[17] At higher voltage the current increases faster than the prediction of the SCLC model.^[20] The occurrence of energetic disorder and corresponding distribution of localized states strongly affects the charge transport properties of conjugated polymers. Assuming a Gaussian density of states (DOS) with width σ , simulations by Bässler linked the occurrence of a temperature- and field dependent mobility in amorphous semiconductors to the presence of disorder.^[21] In this model, the charge transport mechanism is based on hopping of carriers in a Gaussian DOS, and the mobility dependence that was proposed is known as the Gaussian disorder model (GDM). A complication in

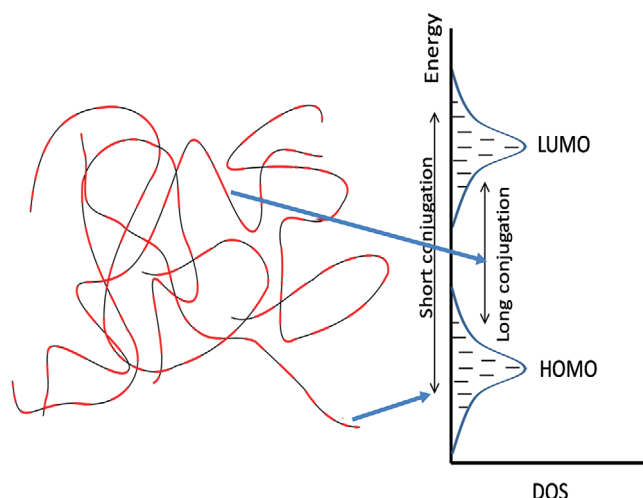


Figure 2. Schematic representation of a disordered conjugated polymer. Differences in conjugation length results in an energetic spreading of the HOMO and LUMO levels of the polymer.

SCLC devices is that with increasing voltage both electric field and charge carrier density are simultaneously increased. In measurements on diodes it is not straightforward to distinguish between the effect of the charge carrier density and the electric field on the mobility. In 2003 Tanase et al. combined diode measurements with field-effect transistor (FET) measurements.^[22] It was found that the measured hole mobility in a FET was orders of magnitudes higher than the one obtained from diode measurements on the same material. The reason is that in a FET the charge carrier density in the conductive channel of a FET is much larger than the typical charge density in diodes, even though the electric field between source and drain is considerably smaller than the electric field in diodes. Therefore, in diodes carriers mainly reside in sites in the tail of the Gaussian DOS, such that a large energy difference has to be overcome by a hop to reach the transport sites close to the center of the DOS. In contrast, in a FET with increasing gate bias and thus increasing density the Fermi-level will move toward the center

of the DOS, such that the energy step for a hopping event is smaller, leading to a higher mobility. By combining the diode and FET data the dependence of charge carrier mobility on density was experimentally determined. Using this dependence, it was subsequently shown that at room temperature in a polymeric SCLC device the hole mobility depends stronger on the charge carrier density than on the electric field.^[23] As a result, care should be taken with reported mobilities, since its value is highly dependent on measurement conditions and device structure. To include also density effects in the charge carrier mobility, Pasveer et al. introduced a model that fully describes the temperature-, field-, and density-dependence of the mobility in disordered semiconductors, also termed the Extended GDM.^[24] The model shows that at higher temperature the density dependence of the mobility becomes more important, whereas at low temperature the field-dependence dominates.

In contrast to the SCL hole current observed in PPV derivatives the electron current is orders of magnitude lower and exhibits a much steeper voltage dependence (see **Figure 3b**).^[17] This observation is a fingerprint for trap-limited transport, indicating the presence of impurities with energetically distributed energy levels in the band gap of the organic semiconductor (Figure 3a).

More recently, for a range of conjugated polymers Nicolai et al. plotted the double logarithmic slope of the electron J - V characteristic as a function of the electron affinity (EA) of the material in the active layer (Figure 6, green squares).^[26] It was observed that with increasing EA, meaning deeper LUMO, the slope and thus steepness of the trap-limited electron current decreases. For polymers with an EA deeper than 3.6 eV, a slope of 2 was obtained, which is a characteristic for the trap-free SCLC. Even more surprising, modeling of the various electron currents using a Gaussian trap distribution demonstrated that the electron transport in the various polymers was dominated by a universal electron trap, energetically centered around 3.6 ± 0.1 eV (below vacuum) with a density of $N_t \approx 3 - 5 \cdot 10^{23} \text{ m}^{-3}$. As origin for a trap with such energy Ho et al. proposed hydrated-oxygen complexes as possible candidate.^[27]

Charge recombination is another important process in PLEDs. The radiative bimolecular recombination process in

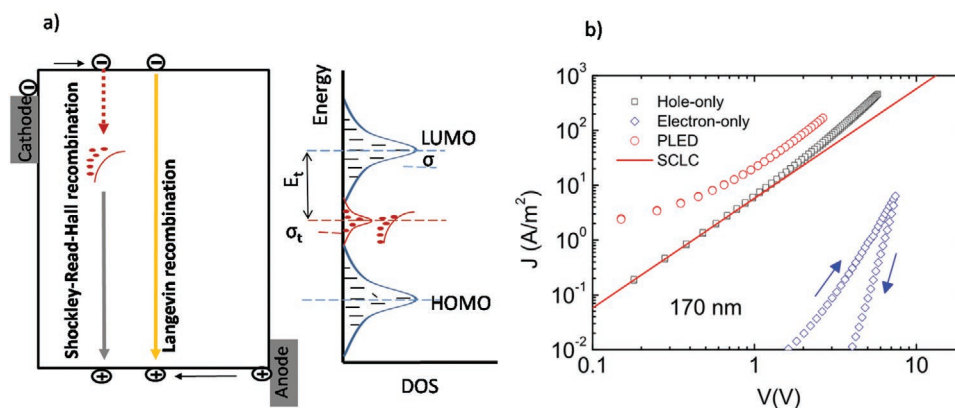


Figure 3. a) Schematic representation of trap-free hole transport and trap-limited electron transport due to energetically distributed electron traps in the band gap. Two types of recombination processes are possible: Radiative Langevin recombination between free carriers and non-radiative Shockley-Read-Hall recombination between trapped-electrons and free holes. b) A plot of the current density versus voltage for a MEH-PPV based hole-only device (black squares), electron-only device (blue diamonds), and PLED dual carrier device (red circles). Reproduced with permission.^[25] Copyright 2019, American Chemical Society.

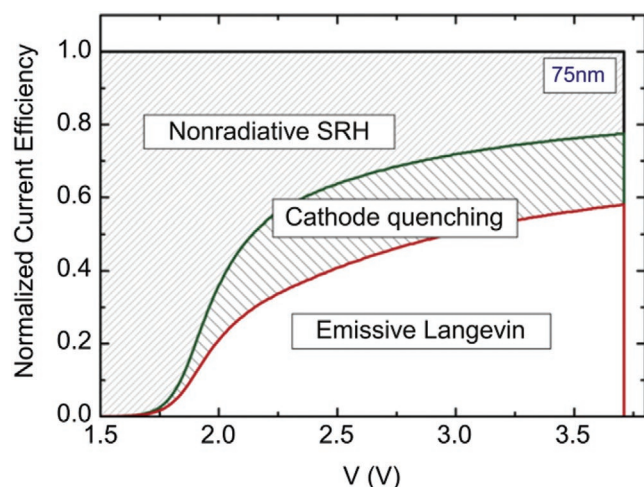


Figure 4. Simulation of contribution of loss effects to the PLED efficiency for a 75 nm MEH-PPV diode as a function of voltage. Reproduced with permission.^[31] Copyright 2012, Elsevier.

conjugated polymers is of the Langevin type,^[28] (Figure 3a), the rate-limiting step is the diffusion of electrons and holes toward each other under the influence of their mutual Coulombic interaction.^[29] However, next to radiative bimolecular Langevin recombination a second non-radiative pathway exists, Shockley-Read-Hall-recombination (SRH recombination), also known as trap-assisted recombination (Figure 3a). The non-radiative SRH recombination is a loss process, with the rate governed by the diffusion of a free hole toward a trapped electron.^[30] Furthermore, due to severe electron trapping most of the recombination takes place close to the cathode. In that case, the bound electron-hole pairs (excitons) will not recombine radiatively, but instead will transfer their energy to the metallic electrode via long range dipole-dipole interactions. The impact of these two loss processes on PLED efficiency has been calculated using a numerical PLED device model. It was found that combination of these processes reduce the PLED efficiency by a factor of two, as shown in **Figure 4**.^[31] This explains why the EQE of fluorescent PLEDs typically amounts to only 1–2% instead of 5%, as would be expected from triplet and outcoupling losses only.

2.2. Recent Developments

2.2.1. Trap-Dilution

Having identified the loss processes in a PLED due to the presence of electron traps, two approaches can be followed to eliminate these losses: The first option is to reduce the negative effects of electron trapping as unbalanced transport and trap-assisted recombination on PLED efficiency. Recently, Abbaszadeh et al. demonstrated an elegant method to nearly eliminate the negative effects of electron traps.^[33] For this, they simultaneously diluted the trapping and transporting sites by mixing the active polymer with an electronically inert large band gap material. The benefit of this trap dilution follows directly from the statistics between free and trapped carriers. Since the

trap-limited current scales with $N_c/N_t^{1/2}$ a simultaneous dilution of transport sites (N_c) and trap sites (N_t) with a factor of ten would for $r = 4$, a typical value for polymeric semiconductors, lead to a thousand times increase of the trap-limited electron current. As shown in **Figure 5**, the trap-limited electron current indeed increased three orders of magnitude for PPV-based blends with 10% active semiconductor and 90% large band gap host. Using trap-dilution they were able to fabricate PLEDs with balanced electron and hole transport and reduced SRH recombination and cathode quenching, leading to the predicted doubling of the efficiency at nearly ten times lower material costs.^[33]

2.2.2. Trap-Free OLEDs

An alternative strategy would be to develop new materials that are intrinsically free of charge carrier trapping. As mentioned above, polymers with an electron affinity higher than 3.6 eV exhibited trap-free electron transport.^[26] As a result, organic semiconductors with sufficiently deep LUMO levels could be attractive candidates for trap-free OLEDs. However, materials with an EA of 3.5 eV or larger will, for visible light-emission, automatically have high ionization energies (HOMO levels) of at least 6 eV. For such an OLED the challenge will shift from electron trapping to hole injection, since injection of holes from known anodes as PEDOT:PSS (work function of 5.1 eV) will be strongly limited due to large injection barriers. Very recently, a simple and robust way of forming an ohmic hole contact on organic semiconductors with high ionization energy (IE) has been proposed.^[34] The injected hole current from high work function metal-oxide electrodes is improved by more than an order of magnitude by using an interlayer, for which the sole requirement is that it has a higher IE than the organic semiconductor. Insertion of the interlayer results in electrostatic decoupling of the electrode from the semiconductor and realignment of the Fermi level with the IE of the organic semiconductor. The ohmic-contact formation is demonstrated for a number of material combinations and solves the problem of hole injection into organic semiconductors with a high IE of up to 6.5 eV. As a result, also hole transport in materials with such high IE could be studied for the first time. In **Figure 6** the slope of the log-log J - V characteristics is shown for a range of organic semiconductors. With regard to the electron transport it was found that films of evaporated small molecules also exhibited trap-limited electron transport as long as their EA is lower than 3.6 eV (Figure 6, red triangles), similar as earlier found for solution-processed conjugated polymers (Figure 6, green squares^[26]). Surprisingly, a similar behavior was found for the hole transport. When the ionization energy of a material surpasses ≈ 6 eV, hole trapping will start to limit the hole transport (figure 6, blue triangles).^[35] As a result, an energy window was identified inside which organic semiconductors do not experience charge trapping for device-relevant thicknesses in the range of 100–300 nm. In this window, the J - V characteristics exhibit the quadratic (slope 2) SCLC behavior, indicative of trap-free transport. When the ionization energy of a material surpasses 6 eV, hole trapping will limit the hole transport, whereas an electron affinity lower than 3.6 eV will give rise to trap-limited electron transport. When both energy levels are within this window, trap-free bipolar charge transport occurs.^[35] To test this design rule further

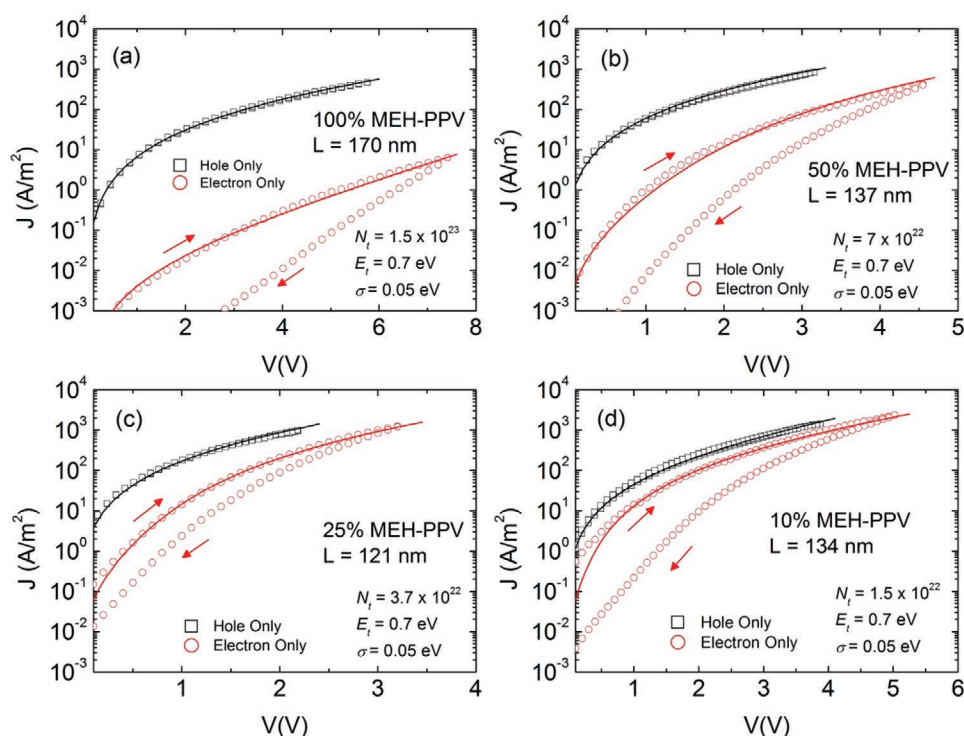


Figure 5. Hole and electron transport in hole-only and electron-only devices of a) MEH-PPV reference device, b) 50:50% MEHPPV:PVK, c) 25:75% MEH-PPV:PVK, and d) 10:90% MEHPPV:PVK wt% blends. The electron trap density in the blends is extracted from numerical simulations (solid lines). Reproduced with permission.^[33] Copyright 2016, Nature Publishing Group.

single layer OLEDs were made from a neat thermally-activated delayed fluorescence emitter with its LUMO and HOMO in the trap-free energy window. It was demonstrated that the absence of trapping as well as the triplet harvesting by TADF results in a high external quantum efficiency of 19%.^[36] This means that the internal quantum efficiency is close to 100%, since ≈80% of the generated light is lost by light outcoupling. Furthermore,

due to the absence of heterojunctions the operating voltage of the single-layer device is exceptionally low, an intensity of 10 000 cd m⁻² is already reached at 2.9 V. An important consequence of this result is that it shows that with regard to efficiency well-designed single layer devices can rival the performance of complex multi-layer devices, opening the route toward efficient fully solution-processed light-emitting devices.

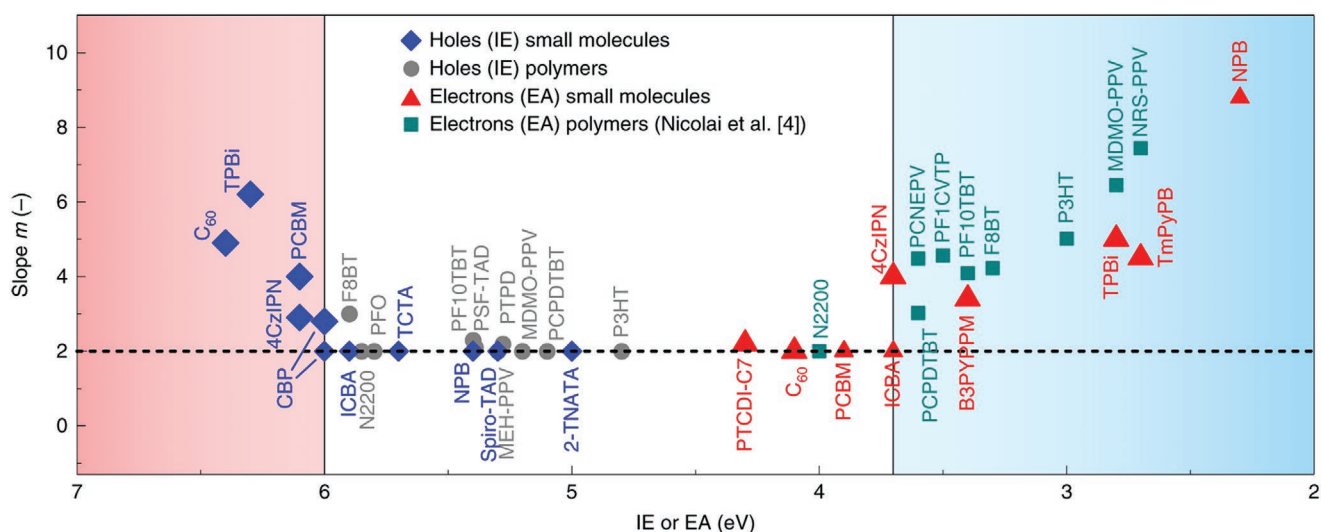


Figure 6. Slope of log J -log V of the hole or electron current versus ionization energy or electron affinity, respectively, for a series of organic semiconductors. An energy window for trap-free charge transport is identified in the range 3.5–6.0 eV. Reproduced with permission.^[35] Copyright 2019, Nature Publishing Group.

2.2.3. PLED Challenges

As shown above, organic TADF semiconductors with energy levels situated within the trap-free energy window lead to efficient light-emitting devices. As a next step, efficient single-layer devices based on TADF polymers will be developed to realize efficient solution-processed PLEDs. However, a limitation is that the energy window has a width of only ≈ 2.5 eV. As a result, for blue-emitting PLEDs with a band gap of 3 eV, removing or disabling charge traps will remain a challenge. The fact that the electron and hole trap centers possess a specific universal energy level leads to the assumption of a common extrinsic origin, such as oxygen- or water-related defects. More work in this direction is required to achieve trap-free blue-emitting organic semiconductors. The major hurdle to still overcome with regard to PLED efficiency is a further enhancement of the optical outcoupling. Incorporation of periodic structures to reduce internal waveguiding enhances the outcoupling efficiency, but often makes organic LEDs more vulnerable to electrical shorts, which is detrimental for large-area devices.^[37,38] Advancement has also been made by preferential orientation of the emitting molecules in the plane of small molecule based multilayer OLEDs.^[39] For single-layer devices, such as PLEDs with a broadened emission zone, so far no significant advancements in optical outcoupling have been reported.

Another important challenge is the operational lifetime of blue-emitting OLEDs. An advantage of single layer OLEDs and PLEDs is that a quantitative study of their degradation mechanisms is more straightforward as compared to complex multilayer structures, which often contain at least five organic layers with eight different compounds. As an example, for single-layer PLEDs based on PPV derivatives it was shown that the voltage drift of a PLED driven at constant current is caused by the formation of hole traps.^[40] The additionally formed hole traps then reduce the PLED light-output by non-radiative recombination between free electrons and trapped holes. As a result, from the voltage increase alone the decay of the light-output can be quantitatively predicted by a numerical PLED device model. Furthermore, from the observation that the rate of hole trap formation scales with the square root of time also the degradation mechanism can be identified. The observed trap formation rate is consistent with exciton-free hole interaction being the main culprit behind PLED degradation.^[40] A direct consequence of this mechanism is that LEDs with a broadened emission zone, meaning locally lower concentrations of excitons and holes, will be more stable than LEDs where the emission zone is confined in a small region. In the above mentioned single-layer trap-free TADF OLED the broadened recombination zone indeed has led to an improved operational stability in comparison with a conventional multilayer OLED structure. Another advantage of using such materials with higher electron affinity is that for electron injection less reactive cathodes can be used, improving the air stability and thus lowering the demands on fabrication and packaging. Further studies on the degradation mechanisms in blue TADF emitters will be carried out in the near future to enhance their stability.

3. Polymer FETs

Next to their application in LEDs conjugated polymers are also interesting materials for organic FET (OFET).^[41] Polymer-based transistors can be the building block for solution-processed electronic circuits that are flexible and lightweight.^[42,43] Furthermore, OFETs can also be used to drive OLEDs as well as for realizing label-free sensing applications.^[44,45] Therefore, intensive efforts both from academic and industry have been made in developing high performance OFETs. A typical OFET device consists of three electrodes (source, drain and gate), a dielectric layer and an active organic semiconducting (OSC) layer (Figure 7a). The selection of source and drain electrodes requires a work function match with the organic semiconductor energy levels. For the dielectric layer, inorganic insulators such as silicon dioxide (SiO_2) or aluminium oxide (Al_2O_3) as well as polymeric insulators such as poly(methyl methacrylate) (PMMA) and cyclized transparent optical polymer are widely used.^[46] The active OSC layer can be deposited by solution processing or thermal evaporation, whose thickness is in the range from a few to hundred nanometers. In OFETs, the charge carrier transport occurs at the interface between the OSC and dielectric layer. OFETs are typically classified into four types, based on the transistor architecture (Figure 7a): bottom-gate and bottom-contact, bottom-gate and top-contact, top-gate and bottom-contact, top-gate and top-contact.^[47,48] For instance, a heavily doped silicon wafer with a 300 nm SiO_2 layer (Si/SiO_2), acting as common-gate electrode and dielectric layer, respectively, is widely used in bottom-gate transistors. The SiO_2 dielectric surface can be modified by a self-assembled monolayer to reduce interfacial traps. Furthermore, the bottom-contact geometry also provides the opportunity to modulate the work function of the electrodes to investigate the charge injection into the active layer. Top-contact devices typically exhibit an improved injection compared to bottom ones and additionally provide the opportunity to observe the interfacial microstructure of the OSC film, which is important to understand the relation between molecular organization, film morphology and charge carrier transport.^[49,50]

3.1. Device Operation of a Polymer FET

To operate a transistor, a bias voltage between source and gate electrodes (V_g) is applied to accumulate charge carriers at the OSC/dielectric interface, combined with a bias voltage between source and drain electrodes (V_{ds}) to drive the transport of these charge carriers along the OSC/dielectric interface (the source electrode is grounded). According to the type of majority charge carriers, there are three types of OFETs, namely p-type, n-type and ambipolar transistors (Figure 7b).^[51,52,53] As explained in the previous section, the type of transport depends on the position of the HOMO and LUMO with regard to the trap-free energy window.^[35] For p-type transistors, a negative V_g drives the accumulation of holes at the OSCs/dielectric interface and a negative V_{ds} (higher than the threshold voltage, V_T) drives the hole transport. For n-type OFETs, accumulation and transport of electrons result from positive V_g and V_{ds} , respectively. In ambipolar OFETs, both holes and electrons can be accumulated and transported at the OSC/dielectric interface.^[51]

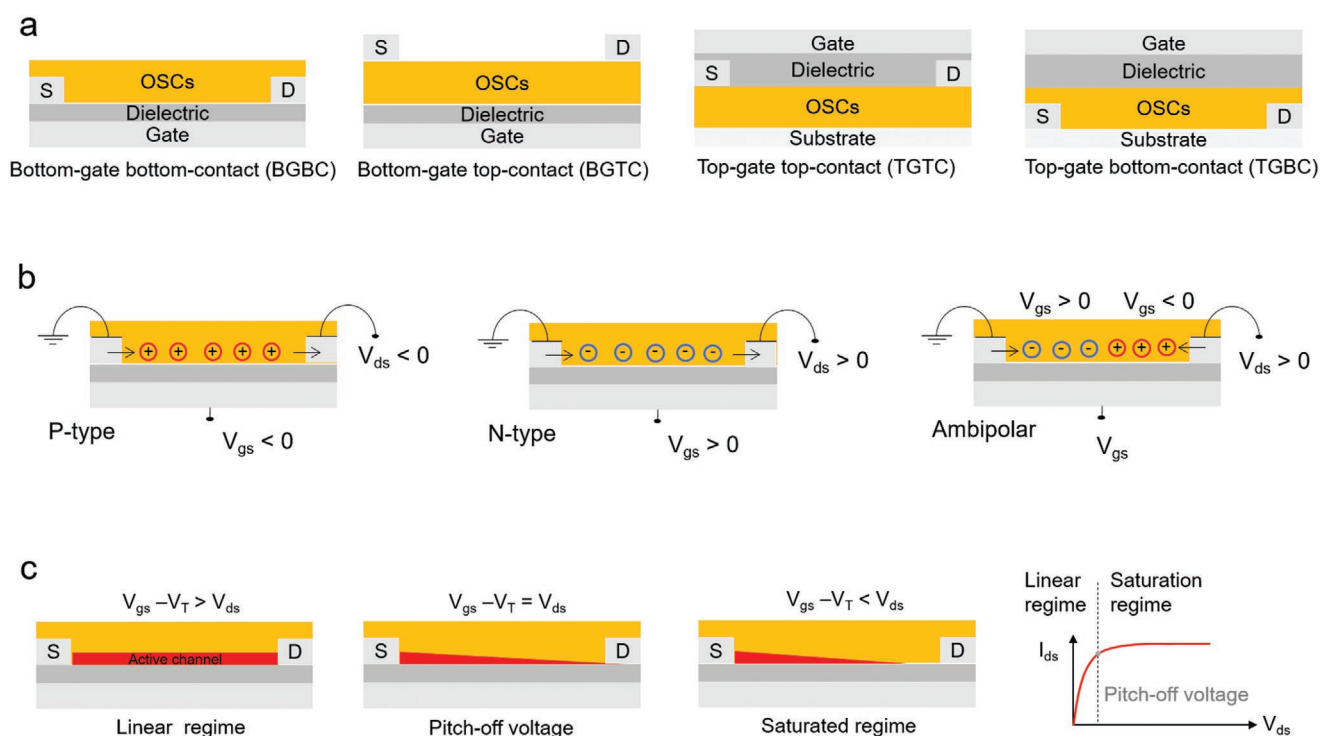


Figure 7. Basic working principles of OFETs. Classification of OFETs based on a) device architecture and b) charge carrier types. c) Linear and saturation regime of OFETs. S and D indicate the source and drain electrodes, respectively.

As discussed above, the combination of V_g and V_{ds} drives the transport of charge carriers. Ideally, only a very low V_g is required to accumulate charge carriers and turn the transistor on. However, in reality, the turn-on of the transistor is affected by trapped charges present at the OSC/dielectric interface. In that case, first a certain V_g is required to overcome the electric field generated by the trapped charges. For larger V_g the additional accumulated carriers contribute to the I_{ds} ($V_g > V_T$). The operation of a transistor is characterized by two regimes, the so-called linear and saturation regime, as shown schematically in Figure 7c. When $V_{ds} = 0$, the accumulated charge carriers uniformly distribute at the OSC/dielectric interface, and $I_{ds} = 0$ since there is no driving voltage. A small V_{ds} ($V_{ds} \ll V_g - V_T$) leads to a linear gradient in charge density from the source to the drain electrode and I_{ds} is proportional to V_{ds} , termed as linear regime. With increasing V_{ds} , a pinch-off appears near the drain electrode at $V_{ds} = V_g - V_T$, forming a charge carrier depletion region. A further increase of V_{ds} will not lead to further enhancement of I_{ds} , termed as saturation regime. In that case, carriers are swept from the pinch-off point to the drain by a comparatively high electric field in the depletion region. A further increase in V_{ds} pushes the pinch-off point further away from the drain ($V_{ds} \gg V_g - V_T$). However, the length of the channel (L) shortens only slightly, as it is infinitely larger than the width of the depletion region, and the integrated resistance of the channel from the source to the pinch point remains more or less the same. For these reasons, once the pinch off condition is met, I_{ds} saturates at $V_{ds} = V_g - V_T$.

The transfer and output curves are the two basic electrical characteristics that evaluate the performance of a transistor.

Figure 8 shows the typical transfer and output curves of a unipolar p-type OFET. The key parameters of an OFET, including charge carrier mobility (μ), on/off ratio, V_T and subthreshold voltage, can all be extracted from the transfer and output curves. As shown in the output curves (Figure 8a), I_{ds} increases with V_{ds} in the linear regime and reaches a stable value in the saturation regime for each V_g . The field effect increases with the applied V_g and leads to a higher I_{ds} . Typical transfer curves for p-type OFETs are shown in Figure 8b. The saturation mobility, threshold and sub-threshold can be estimated from the slope of $(I_{ds})^{1/2}$ - V_g and I_{ds} - V_g curves, respectively.

Dependent on the temperature-dependence of the mobility in OFETs, the charge transport mechanism is either classified into band (-like) transport (mobility increases with decreasing temperature) or hopping regime (mobility decreases with decreasing temperature). In the hopping regime, the charge carrier transport is typically thermally activated, where the charge carrier mobility increases with temperature and carrier density due to filling of the density of states, which is broadened by disorder.^[54,55] Next to the energetic disorder, as schematically indicated in Figure 2, in OFETs also structural disorder due to differences in morphology and packing of the molecules/polymers plays an important role in their charge transport properties. The presence of inherent disorder and thermally-activated structural fluctuations pose a fundamental challenge to the realization of band(-like) transport. Therefore, in most cases, polycrystalline and amorphous OSCs exhibit hopping dominated transport.^[41] Band(-like) transport is observed only in a very limited number of systems, as in conjugated polymers with extremely low torsion in the chains.^[56,57] The presence

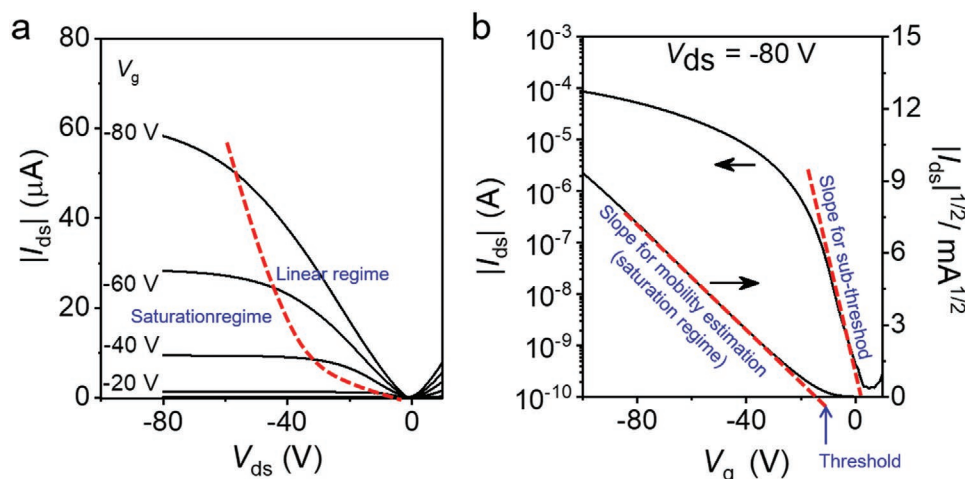


Figure 8. Characterization of p-type OFETs by a) output and b) transfer curves.

of interfacial traps significantly influences the charge carrier transport in OFETs.^[58] Chua et al.^[59] investigated the transfer curves of an n-type transistor using the polymer poly(9,9-dioctylfluorene-alt-benzothiadiazole) as semiconductor on different substrate interfaces, such as a bare Si/SiO₂ substrate (*S_{bare}*), Si/SiO₂ substrate modified with a hexamethyldisilazane (HMDS) self-assembled monolayer (*S_{HMDS}*), dodecyltrichlorosilane (DTS) modified substrate (*S_{DTS}*), trichloro(octadecyl)silane (OTS) modified substrate (*S_{OTS}*) and polyethylene substrate (*S_{PE}*). They demonstrated that the channel current *I_{ds}* gradually increased, when going from *S_{bare}* to *S_{HMDS}* and *S_{OTS}* and *S_{PE}*, accompanied by a gradual decrease of *V_T*. As a result, self-assembled monolayers can be used to reduce but not completely eliminate traps at or near the SiO₂ interface.^[59] In addition to the interfacial traps, also bulk traps that originate from molecular disorder and grain boundaries impede the charge transport.

3.2. Performance and Stability of Polymer FETs

For polymer-based FETs the mobility is determined by the charge carrier transport along and between polymer chains. Molecular regioregularity, molecular weight, polydispersity, rotational freedom along the conjugated backbone and the construction of donor-acceptor conjugated systems are important factors that influence charge carrier transport. Most organic thin film transistors are based on semi-crystalline and/or amorphous OSCs. For instance, semi-crystalline polymer OSCs consist of ordered and disordered regions, as shown in **Figure 9a**. The ordered region exhibits strong π - π stacking and long-range periodicity, where the charge carrier transport depends on molecule packing orientation and π - π stacking distance.^[60] In contrast to ordered regions, disordered regions are governed by weak intermolecular interactions limiting π - π stacking and/or interlayer packing. The main transport pathways for charge carriers

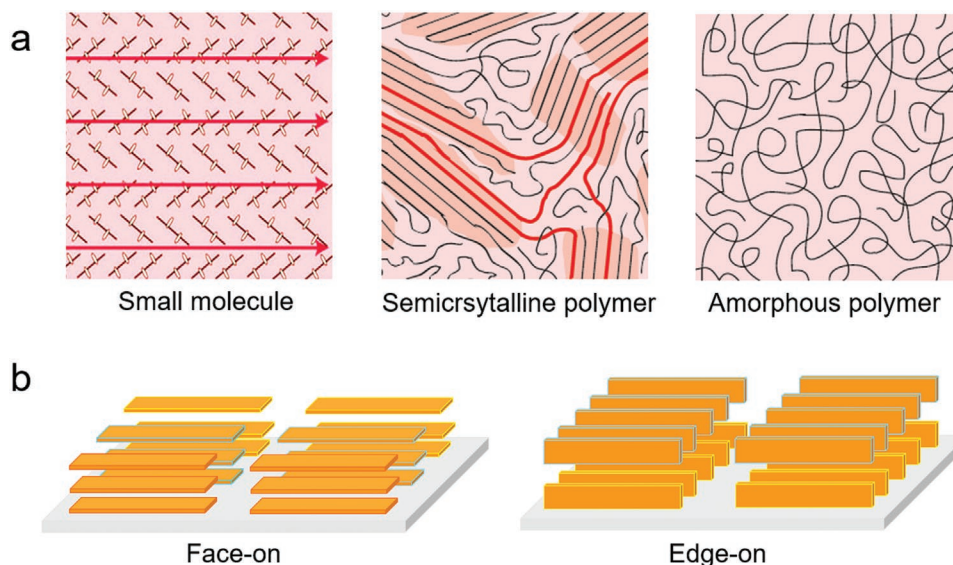


Figure 9. a) Charge transport and molecular microstructure in different OSCs.^[57,58] Reproduced with permission.^[61] Copyright 2013, Nature Publishing Group. b) Illustration of face-on and edge-on of polymer OSCs.

in disordered region are over the polymer chains (Figure 9a). Therefore, the charge transport in the ordered region of semi-crystalline OSCs is higher than in the amorphous parts and the connections between the ordered regions play a dominate role on charge carrier transport over macroscopic dimensions.^[61] In contrast to semi-crystalline polymer OSCs, amorphous polymer OSCs only show a disordered region and exhibit a limited charge transport performance due to weak intermolecular interactions (Figure 9a). The molecular organization of ordered polymer OSCs refers to the molecular packing orientation and packing distance. According to the molecular packing orientation toward the substrate surface, thin film OSCs are classified into edge-on and face-on.^[62] In the case of edge-on organization, the backbone plane is arranged perpendicular to the substrate so that the π -stacking direction is oriented parallel to the substrate surface, favorable for charge carrier transport in OFETs. In contrast, in the face-on orientation the backbone plane is parallel to substrate and the π -stacking direction is perpendicular to the substrate (Figure 9b).^[47] A face-on arrangement often leads to lower field-effect mobilities in OFETs, but might be favorable for solar cell cells.^[63] Common conjugated polymers applied in OFETs include polythiophene^[64] and various donor-acceptor polymers.^[65] Among polymer OSCs, donor-acceptor polymers typically exhibit field-effect mobilities on the order of $10^{-2} - 1 \text{ cm}^2 \text{ V}^{-1} \text{ s}^{-1}$, but several examples showed a mobility over $10 \text{ cm}^2 \text{ V}^{-1} \text{ s}^{-1}$.^[65] It should be noted that for high mobility OFETs the effects of contact resistance should be correctly taken into account in order not to overestimate the mobility.^[66] Next to the development of high mobility p-type transistors also progress has been made for n-type semiconductors. A well-known example is

poly{[N,N'-bis(2-octyldodecyl)-naphthalene-1,4,5,8-bis(dicarboximide)-2,6-diyl]-alt-5,5'-(2,2'-bithiophene)}, also known as N2200.^[67] By optimization of processing spin-coating conditions that introduce pre-aggregation in solution mobilities in excess of $1 \text{ cm}^2 \text{ V}^{-1} \text{ s}^{-1}$ have been obtained.^[68] Using wire-bar coating the mobility was even further enhanced to $6.4 \text{ cm}^2 \text{ V}^{-1} \text{ s}^{-1}$ by inducing highly ordered elongated nanostructures.^[69]

Another important development has been the development of ultrathin gate dielectric layers in order to lower the operating voltages of OFETs. In one approach, a thin hybrid organic/inorganic gate dielectric was applied consisting of a thin (3.6 nm) layer of aluminum oxide (AlOx) layer covered with a self-assembled monolayers of n-tetradecylphosphonic acid (1.7 nm), resulting in a gate dielectric with a total thickness of 5.3 nm and a capacitance of 600 nF cm^{-2} .^[70] In another approach, self-assembled nanodielectrics were developed, consisting of self-assembled multilayers by spontaneous adsorption of active molecular precursor(s) onto solid surfaces, leading to ordered molecular assemblies.^[71] In this approach the thickness and related insulating properties and transparency can be tuned.

Next to a steady increase in charge carrier mobility also achieving improved electrical stability of polymer-based FETs is a prerequisite for commercialization. Especially for applications that continuously require current, such as transistors driving an OLED in a display, the so-called current bias stress is a major challenge. A shift of the threshold voltage ΔV_{th} as a result of bias stress modifies the transistor current and therefore also

the pixel brightness. For application in OLED displays a typical requirement for organic transistors is that $\Delta V_{th} < 1 \text{ V}$ for 100 h of constant current bias stress at room temperature.^[41] As mentioned above, threshold voltage shifts ΔV_{th} originate from trapped charges, either in the bulk of the semiconductor, at the semiconductor-dielectric interface, or at grain boundaries.^[72,73] Consequently, the stability of the threshold voltage depends on the individual materials in the OFET as well on the interfaces and the processing. Furthermore, additional trap states might be formed by external impurities such as water and oxygen, similar as discussed for the PLEDs. In a recent study, solution-processed organic FETs were presented exhibiting excellent stability, even under ambient conditions.^[74] As shown in Figure 10, the observed bias stress stability of the OFET even exceeds the stability of FETs based on competing technologies as a-Si and IGZO. The excellent stability, combined with a high mobility of $3 \text{ cm}^2 \text{ V}^{-1} \text{ s}^{-1}$ and high on/off ratio of 10^6 demonstrates that polymer based FETs now have reached the requirements for commercialization in flexible backplanes.

4. Organic Electrochemical Transistors

4.1. PEDOT:PSS

Electronic devices mainly rely on electrons as the dominant charge carriers, whereas in biology this is rarely the case. Instead, ions and small molecules are being used.^[75,76] Since conjugated polymers can be designed to offer mixed electronic and ionic conductivity, these materials can provide highly

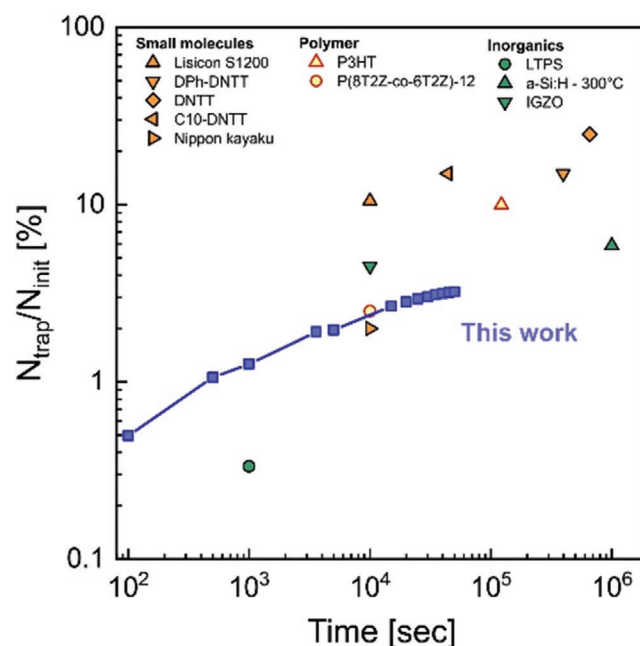


Figure 10. Comparison of the bias stress stability of OFETs based on a p-type semiconducting polymer (blue squares) devices to other highly stable semiconductors that exhibit good bias stress stability. N_{trap}/N_{init} represents the ratio of the trapped charge density (N_{trap}) and initial mobile charge carrier density N_{init} . Reproduced with permission ^[74] Copyright 2019, Wiley-VCH.

efficient signal transduction and amplification between those fields.^[77] Furthermore, a beneficial property of (semi)conducting polymers is that their soft nature mimics the mechanical properties biological systems. Materials such as the conducting polymer poly(3,4-ethylenedioxythiophene) (PEDOT), doped with poly(styrene sulfonic acid) (PSS), were found to perform very well in a biological environment.^[78,79] Besides its insolubility, PEDOT stands out with its high electro-optical and electrical properties, featuring hole conductivities of $1\text{--}100\text{ S cm}^{-1}$.^[79,80] Its conductivity strongly depends on the morphology and the dopant. Traditionally, it is doped with the water-soluble polyelectrolyte PSS, which makes the blend PEDOT:PSS water-dispersible. The polarity of the sulfonate groups enables PSS to solvate the PEDOT, leading to stable aqueous dispersions.^[80,81] The structure of PEDOT:PSS consists of PEDOT-rich particles with a size of 20–25 nm in diameter, surrounded by PSS-rich lamellas in excess.^[82] The composition is typically described as gel-like particles, embedded in PSS shells to stabilize the dispersion. The long shelf-life facilitates a variety of commercially available PEDOT:PSS formulations (e.g., Hereaus Clevios, Sigma Aldrich), which are ready-for-use without any further instructions.^[83] Surfactant are often added to the PEDOT:PSS dispersion to enhance the wetting behavior, giving improved film formation on hydrophobic substrates. The fluorosurfactant Zonyl is often used for this purpose.^[84] Adding crosslinkers as 3-glycidoxypolytrimethoxysilane (GOPS) to PEDOT:PSS reduces its ability to absorb water, which reduces swelling of the film.^[85,86] Despite the attractive properties as enhanced stability, the addition of a crosslinker, however, also lowers the conductivity and the ion mobility, which basically implies a trade-off between mechanical stability and electrical performance.^[85] The electronic conductivity of PEDOT:PSS films have been extensively studied under several conditions, involving additives, solvents, surfactants and processing methods.^[87] In fact, various physical and chemical approaches, commonly defined as secondary doping, have been used to improve the electrical conductivity of PEDOT:PSS. In this way, the conductivity of commercially obtainable PEDOT:PSS films (pristine) of $10^{-6} - 1\text{ S cm}^{-1}$ can be increased several orders of magnitude, reaching a maximum value in excess of 4000 S cm^{-1} .^[87] Treatment with high boiling organic solvents is the most prominent

technique to enhance PEDOT:PSS conductivity.^[86] The enhancement in PEDOT:PSS conductivity by *secondary doping* is induced by a structural rearrangement and loss of the excess, insulating PSS.^[87,88,89]

4.2. Polymer Electrochemical Transistor

PEDOT:PSS is typically used as the active layer in one of the most promising devices for biosensing employing mixed ionic-electric conduction, the organic electrochemical transistor (OECT). Here, ions are injected from an electrolyte into the conducting polymer by a gate bias, thereby modulating its hole conductivity. In 1984 the first OECT was introduced by Wrighton and his colleagues, as a new class of an electrolyte-gated organic field-effect transistors.^[90] The OECT consists of a (semi)conducting polymer, horizontally sandwiched between two metal electrodes (**Figure 11**), acting as the source and the drain.^[91] The application of a drain voltage V_D induces a current (drain current, I_D), which flows from source to drain and is proportional to the number of mobile holes or electrons in the conducting channel. The conducting polymer is in direct contact with an electrolyte, in this example sodium chloride, in which a gate electrode is immersed. Upon application of a gate bias V_G ions are injected from the electrolyte into the conducting polymer, modifying its doping state, and thereby its bulk conductivity. In this way, V_G regulates the doping state of the conducting polymer, while V_D probes the doping state of the channel. In case of electrolyte gated organic FETs ions cannot penetrate the semiconductor, here upon applying a gate bias charges in the semiconductor are induced that nearly compensate the interface charge of the electrolyte.

The PEDOT:PSS-based OECT operates in the depletion mode. Driven by the electric field of the gate electrode, cations of the electrolyte are able to penetrate the channel and compensate the negative charges of the sulfonate groups of PSS.^[91] This migration causes an electrochemical dedoping of PEDOT. The highly conductive oxidized PEDOT⁺ will be reduced to the less conductive neutral state (PEDOT⁰), according to the following reversible electrochemical reaction^[79]

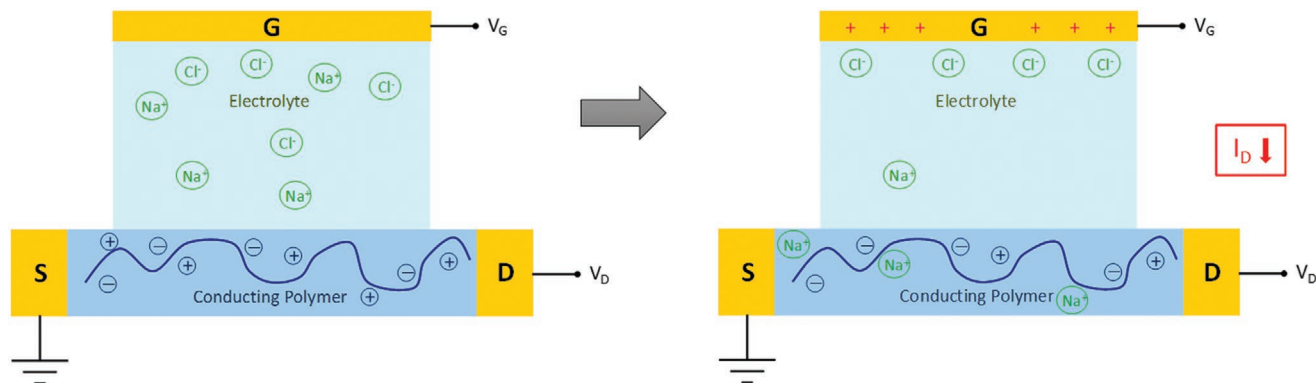


Figure 11. Operation of an OECT: Typical device structure of an OECT, consisting of a source (S), drain (D) connected by a conducting polymer and a gate (G), which in this example is immersed in a NaCl electrolyte. Upon application of a positive gate bias positive Na⁺ ions penetrate into the conducting polymer, replacing the mobile holes leading to a reduction of the current between source and drain.

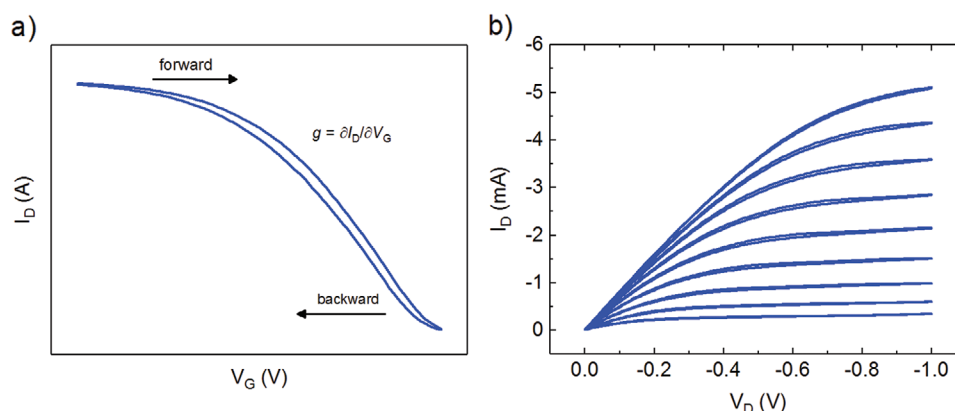


Figure 12. OECT characteristics operating in the depletion mode: a) Transfer characteristics show the forward and backward sweep of I_D at a specific V_D , revealing the hysteresis of the device. b) Output characteristics for a series of V_G , displaying the transition from linear to saturation regime.



where M^+ is a cation of the electrolyte and e^- an electron from the source. In other words, the number of mobile holes is replaced by immobile ions in the channel, which results in a lowering of the hole current. The transistor is pushed into the off-state (I_D is decreased) due to the decreased hole density. This process is reversible and recovers by ions drifting back to the electrolyte.^[79] As a result, in contrast to traditional OTFTs, the drain current (I_D) is regulated by electrochemical reactions in the channel. This makes the OECT an efficient ion-to electron transducer.

The electrical behavior of an OECT is represented by its current-voltage (I - V) characteristics.^[73] The transfer characteristics of a OECT operating in depletion mode in **Figure 12a**, show the modulation of I_D according to the dedoping (forward sweep) and doping (backward sweep) process of the channel, regulated by V_G . Due to the coupling of ionic and electronic charges throughout the entire volume of the channel OECTs exhibit one of the highest transconductances among different types of transistors.^[91] Defined as $g_m = \partial I_D / \partial V_G$, the transconductance is the first derivative of the transfer curve, highlighting the efficiency of the transduction of the input/output signal. OECTs typically reach a transconductance in the range of millisiemens.^[91] It has recently been found that the ion penetration strongly depends on hydration of the conducting polymer as well as its nanoscale morphology.^[92] As an example, enhancing the crystallinity of the polymer by thermal annealing on one hand increases the OFET mobility but also decreases the mobility of ions in the OECT.

Bernards et al. established an OECT device model, which describes the steady-state and transient behavior of the OECT.^[93] The model incorporates an ionic and electronic circuit and fits the output characteristics well, allowing for an estimation of essential characteristics such as charge carrier mobility and density. Similar to an OFET, the OECT can operate in the linear or saturation regime, depending on the applied gate and drain voltages. In the output characteristics (Figure 12b) the transition from the linear to the saturation regime is clearly displayed. In the linear regime the dedoping is homogenous throughout the organic polymer, whereas in saturation the channel is completely dedoped close to the drain side (pinched-off) and I_D is almost independent on V_D .^[93]

Due to the very low operating voltages, its biocompatibility and the ease of fabrication, OECTs are suited for a broad range of applications, including logic circuits, memory and neuro-morphic devices, and bioelectronic devices.^[94] Due to the soft nature of the conducting polymer and development of soft, flexible and stretchable substrates, OECTs play a major role in bioelectronics for biomedical and healthcare related usage and show high potential toward clinical applications. High sensitivity and excellent signal-to-noise ratio provides the OECT with the ability to monitor cell activity when integrated with electrically active tissues and organs.^[94–96] Implantable devices have been placed for example on the brain of a rat to record epileptic seizures.^[97] Hence, OECTs are able to provide amplified recordings of electrophysiological signals from the brain, heart, and other organs.^[94] For cutaneous application, it is possible to record electrocardiograms when placed in contact with the human skin.^[98] In addition, the OECT can monitor the action potential of electrogenic cells to provide a spatial map of the electrophysiological activity.^[99] OECTs have also been used for cell culture analysis, as well as cell membrane integrity for non-electrogenic cells, for both in vitro and in vivo applications.^[100,101] Furthermore, OECTs have been used to monitor ion transport through cellular barriers via the paracellular pathway.^[102] By using OECTs in a current-driven mode their ion sensitivity normalized to the supply voltage can be strongly enhanced, reaching to record values of up to $1200 \text{ mV V}^{-1} \text{ dec}^{-1}$, which exceeds the Nernst limit by one order of magnitude.^[103] Rupturing the integrity of CaCo-2 cell barriers by H_2O_2 was monitored by the change of the output voltage in the transfer characteristics of OECTs in the current-driven configuration.^[104] Furthermore, OECTs have been successfully used as a transducer to detect different electrolytes and metabolites.^[105–110] This includes in particular glucose and lactate, which are important for human health, as lactate states the metastatic potential of tumor cells.^[106,107,111] In addition to the detection of an analyte in a saline solution, also sensing in breath, saliva, sweat and cell culture media has been accomplished.^[112–114]

Finally, there is a great interest in developing networks for information processing and transmission, as well as recognition and storage based on OECTs, inspired by the inherent capability of the human brain to cope with this kind of signals.

Neuromorphic systems are devices that mimic the structure and function of biological neural networks, to be able to recognize temporary or permanent changes in electrical signals, and thereby simulating short-term or long-term memory.^[115] The OECT has been used in a variety of neuromorphic and memory devices, especially owing to its low power consumption per switching event.^[115–117] Furthermore, it was demonstrated that in an array of OECTs connected through a common electrolyte the output of these devices can be synchronized by a global oscillatory input, similar as how global oscillations in the brain synchronize neural populations, paving the way to novel neuromorphic architectures.^[118]

5. Conclusion

During the past three decades, semiconducting polymers have been investigated intensively for use in electronic devices as light-emitting diodes, photovoltaic cells, field-effect transistors, and sensors. Crucial for efficient device operation are the charge-transport properties of both holes and electrons. The electron transport in typical semiconducting polymers is often found to be orders of magnitude lower than the hole transport due to trapping. The electron trap depths appear to be directly related to the electron affinity of the polymer, revealing that the polymers exhibit a common trap distribution related to oxygen/water complexes. As first step toward devices with balanced and trap-free transport is by dilution of the transport and trapping sites of a semiconductor, leading to a doubling of the PLED efficiency. Furthermore, an energy window for trap-free electron and hole transport was recently found, serving as a design rule for future polymeric semiconductors. Combined with thermally-activated delayed fluorescence it has been demonstrated that also organic LEDs based on a single active layer exhibits high efficiency, opening a route toward efficient printed polymer LEDs. With regard to polymeric transistors large progress in bias/current stress has been reported, even in ambient atmosphere. Furthermore, conducting polymers have recently emerged as candidates for biosensing and neuromorphic computing, due to their ability to conduct both ionic and electronics carriers, which enables them to operate in electrolytes as encountered in a biological environment. A remaining challenge is now to fully eliminate the remaining effects of external defects as oxygen and water in order to exploit the promising intrinsic properties of semiconducting polymers.

Acknowledgements

This article is part of the Advanced Materials Technologies Hall of Fame article series, which recognizes the excellent contributions of leading researchers to the field of technology-related materials science. The author would like to thank all his former and present colleagues at the University of Groningen and Max Planck Institute for Polymer Research, respectively, for their contributions to the presented work.

Conflict of Interest

The author declares no conflict of interest.

Keywords

light-emitting diodes, organic electronics, semiconducting polymers, sensors, transistors

Received: February 20, 2020

Revised: March 30, 2020

Published online:

- [1] C. K. Chiang, C. R. Fincher Jr., Y. W. Park, A. J. Heeger, H. Shirakawa, E. J. Louis, S. C. Gau, A. G. MacDiarmid, *Phys. Rev. Lett.* **1977**, 39, 1098.
- [2] J. H. Burroughes, D. D. C. Bradley, A. R. Brown, R. N. Marks, K. Mackay, R. H. Friend, P. L. Burns, A. B. Holmes, *Nature* **1990**, 347, 539.
- [3] M. Fleuster, M. Klein, P. Roosmalen, A. Wit, H. Schwab, *SID Symp. Digest Techn. Papers* **2004**, 35, 1276.
- [4] C. J. Drury, C. M. J. Mutsaerts, C. M. Hart, M. Matters, D. M. de Leeuw, *Appl. Phys. Lett.* **1998**, 73, 108.
- [5] C. J. Brabec, N. S. Sariciftci, J. C. Hummelen, *Adv. Funct. Mater.* **2001**, 11, 15.
- [6] B. Adhikari, S. Majumdar, *Prog. Polym. Sci.* **2004**, 29, 699.
- [7] C. W. Tang, S. A. Van Slyke, *Appl. Phys. Lett.* **1987**, 51, 913.
- [8] J. Kido, M. Kimura, K. Nagai, *Science* **1995**, 267, 1332.
- [9] J. Kwon, R. Pode, in *Organic Light Emitting Diode—Material, Process, and Devices* (Ed: S. H. Ko), IntechOpen, London **2011**.
- [10] M. A. Baldo, D. F. O'Brien, Y. You, A. Shoustikov, S. Sibley, M. E. Thompson, S. R. Forrest, *Nature* **1998**, 395, 151.
- [11] C. Adachi, M. A. Baldo, M. E. Thompson, S. R. Forrest, *J. Appl. Phys.* **2001**, 90, 5048.
- [12] H. Uoyama, K. Goushi, K. Shizu, H. Nomura, C. Adachi, *Nature* **2012**, 492, 234.
- [13] Q. Zhang, B. Li, S. Huang, H. Nomura, H. Tanaka, C. Adachi, *Nat. Photonics* **2014**, 8, 326.
- [14] R. Meerheim, B. Lussem, K. Leo, *Proc. IEEE* **2009**, 97, 1606.
- [15] I. Campbell, P. S. Davids, D. Smith, N. Barashkov, J. Ferraris, *Appl. Phys. Lett.* **1998**, 72, 1863.
- [16] Y. Shen, A. R. Hosseini, M. H. Wong, G. G. Malliaras, *ChemPhys-Chem* **2004**, 5, 16.
- [17] P. W. M. Blom, M. J. M. de Jong, J. J. M. Vleggaar, *Appl. Phys. Lett.* **1996**, 68, 3308.
- [18] N. F. Mott, R. W. Gurney, *Electronic Processes in Ionic Crystals*, Oxford University Press, Oxford **1940**.
- [19] M. Van der Auweraer, F. C. De Schryver, P. M. Borsenberger, H. Bässler, *Adv. Mater.* **1994**, 6, 199.
- [20] P. W. M. Blom, M. J. M. de Jong, M. G. Van Munster, *Phys. Rev. B* **1997**, 55, R656.
- [21] H. Bässler, *Phys. Status Solidi B* **1993**, 175, 15.
- [22] C. Tanase, E. J. Meijer, P. W. M. Blom, D. M. de Leeuw, *Phys. Rev. Lett.* **2003**, 91, 216601.
- [23] C. Tanase, P. W. M. Blom, D. M. de Leeuw, *Phys. Rev. B* **2004**, 70, 193202.
- [24] W. F. Pasveer, J. Cottaar, C. Tanase, R. Coehoorn, P. A. Bobbert, P. W. M. Blom, D. M. de Leeuw, M. A. J. Michels, *Phys. Rev. Lett.* **2005**, 94, 206601.
- [25] D. Abbaszadeh, A. Kunz, N. B. Kotadiya, A. Mondal, D. Andrienko, J. J. Michels, G.-J. A. H. Wetzelaer, P. W. M. Blom, *Chem. Mater.* **2019**, 31, 6380.
- [26] H. T. Nicolai, M. Kuik, G. A. H. Wetzelaer, B. de Boer, C. Campbell, C. Risko, J. L. Bredas, P. W. M. Blom, *Nat. Mater.* **2012**, 11, 882.
- [27] J. M. Zhuo, L. H. Zhao, R. Q. Png, L. Y. Wong, P. J. Chia, J. C. Tang, S. Sivaramakrishnan, M. Zhou, E. C. W. Ou, S. J. Chua, W. S. Sim, L. L. Chua, P. K. H. Ho, *Adv. Mat.* **2009**, 21, 4747.

- [28] U. Albrecht, H. Bässler, *Phys. Status Solidi B* **1995**, 191, 455.
- [29] P. Langevin, *Ann. Chim. Phys.* **1903**, 28, 122.
- [30] M. Kuik, L. J. A. Koster, G. A. H. Wetzelaer, P. W. M. Blom, *Phys. Rev. Lett.* **2011**, 107, 256805.
- [31] M. Kuik, L. J. A. Koster, A. Dijkstra, G.-J. A. H. Wetzelaer, P. W. M. Blom, *Org. Electron.* **2012**, 13, 969.
- [32] P. Mark, W. Helfrich, *J. Appl. Phys.* **1962**, 33, 205.
- [33] D. Abbaszadeh, A. Kunz, G.-J. A. H. Wetzelaer, J. J. Michels, N. I. Crăciun, K. Koynov, I. Lieberwirth, P. W. M. Blom, *Nat. Mater.* **2016**, 15, 628.
- [34] N. B. Kotadiya, H. Lu, A. Mondal, Y. Ie, D. Andrienko, P. W. M. Blom, G.-J. A. H. Wetzelaer, *Nat. Mater.* **2018**, 17, 329.
- [35] N. B. Kotadiya, A. Mondal, P. W. M. Blom, D. Andrienko, G.-J. A. H. Wetzelaer, *Nat. Mater.* **2019**, 18, 1182.
- [36] N. B. Kotadiya, P. W. M. Blom, G.-J. A. H. Wetzelaer, *Nat. Photonics* **2019**, 13, 765.
- [37] Y. Sun, S. R. Forrest, *Nat. Photonics* **2008**, 2, 483.
- [38] Y. Li, M. Kovačič, J. Westphalen, S. Oswald, Z. Ma, C. Hänisch, P.-A. Will, L. Jiang, M. Junghaehnel, R. Scholz, S. Lenk, S. Reineke, *Nat. Commun.* **2019**, 10, 2972.
- [39] T. D. Schmidt, Th. Lampe, D. Sylvinson, M. R. , P. I. Djurovich, M. E. Thompson, W. Brütting, *Phys. Rev. Appl.* **2017**, 8, 037001.
- [40] Q. Niu, R. Rohloff, G. A. H. Wetzelaer, P. W. M. Blom, N. I. Crăciun, *Nat. Mater.* **2018**, 17, 557.
- [41] H. Sirringhaus, *Adv. Mater.* **2014**, 26, 1319.
- [42] S. J. Benight, C. Wang, J. B. H. Tok, Z. Bao, *Prog. Polym. Sci.* **2013**, 38, 1961.
- [43] Y. Yao, H. Dong, W. Hu, *Adv. Mater.* **2016**, 28, 4513.
- [44] T. Someya, Z. Bao, G. G. Malliaras, *Nature* **2016**, 540, 379.
- [45] T. Lei, M. Guan, J. Liu, H. C. Lin, R. Pfattner, L. Shaw, A. F. McGuire, T. C. Huang, L. Shao, K. T. Cheng, J. B. H. Tok, Z. Bao, *Proc. Natl. Acad. Sci. USA* **2017**, 114, 5107.
- [46] D. Khim, Y. Xu, K. J. Baeg, M. Kang, W. T. Park, S. H. Lee, I. B. Kim, J. Kim, D. Y. Kim, C. Liu, Y. Y. Noh, *Adv. Mater.* **2016**, 28, 518.
- [47] A. Salleo, *Mater. Today* **2007**, 10, 38.
- [48] A. Facchetti, *Mater. Today* **2007**, 10, 28.
- [49] X. Guo, M. Baumgarten, K. Müllen, *Prog. Polym. Sci.* **2013**, 38, 1832.
- [50] Y. Diao, L. Shaw, Z. Bao, S. C. B. Mannsfeld, *Energy Environ. Sci.* **2014**, 7, 2145.
- [51] E. C. P. Smits, T. D. Anthopoulos, S. Setayesh, E. van Veenendaal, R. Coehoorn, P. W. M. Blom, B. de Boer, D. M. de Leeuw, *Phys. Rev. B* **2006**, 73, 205316.
- [52] K. Zhou, H. Dong, H. L. Zhang, W. Hu, *Phys. Chem. Chem. Phys.* **2014**, 16, 22448.
- [53] R. Schmechel, M. Ahles, H. von Seggern, *J. Appl. Phys.* **2005**, 98, 084511.
- [54] M. C. J. M. Vissenberg, M. Matters, *Phys. Rev. B* **1998**, 57, 12964.
- [55] E. J. Meijer, C. Tanase, P. W. M. Blom, E. Van Veenendaal, B.-H. Huisman, D. M. de Leeuw, T. M. Klapwijk, *Appl. Phys. Lett.* **2002**, 80, 3838.
- [56] D. Venkateshvaran, M. Nikolka, A. Sadhanala, V. Lemaure, M. Zelazny, M. Kepa, M. Hurhangee, A. J. Kronemeijer, V. Pecunia, I. Nasrallah, I. Romanov, K. Broch, I. McCulloch, D. Emin, Y. Olivier, J. Cornil, D. Beljonne, H. Sirringhaus, *Nature* **2014**, 515, 384.
- [57] Y. Yamashita, J. Tsurumi, F. Hinkel, Y. Okada, J. Soeda, W. Zajackowski, M. Baumgarten, W. Pisula, H. Matsui, K. Müllen, J. Takeya, *Adv. Mater.* **2014**, 26, 8169.
- [58] Y. Don Park, J. A. Lim, H. S. Lee, K. Cho, *Mater. Today* **2007**, 10, 46.
- [59] L. L. Chua, J. Zaumseil, J. F. Chang, E. C. W. Ou, P. K. H. Ho, H. Sirringhaus, R. H. Friend, *Nature* **2005**, 434, 194.
- [60] E. J. Crossland, K. Tremel, F. Fischer, K. Rahimi, G. Reiter, U. Steiner, S. Ludwigs, *Adv. Mater.* **2012**, 24, 839.
- [61] R. Noriega, J. Rivnay, K. Vandewal, F. P. Koch, N. Stingelin, P. Smith, M. F. Toney, A. Salleo, *Nat. Mater.* **2013**, 12, 1038.
- [62] M. S. Chen, J. R. Niskala, D. A. Unruh, C. K. Chu, O. P. Lee, J. M. J. Fréchet, *Chem. Mater.* **2013**, 25, 4088.
- [63] M. Li, C. An, T. Marszalek, M. Baumgarten, H. Yan, K. Müllen, W. Pisula, *Adv. Mater.* **2016**, 28, 9430.
- [64] I. McCulloch, M. Heeney, C. Bailey, K. Genevicius, I. MacDonald, M. Shkunov, D. Sparrowe, S. Tierney, R. Wagner, W. Zhang, M. L. Chabinyc, R. J. Kline, M. D. McGehee, M. F. Toney, *Nat. Mater.* **2006**, 5, 328.
- [65] Y. Yamashita, F. Hinkel, T. Marszalek, W. Zajackowski, W. Pisula, M. Baumgarten, H. Matsui, K. Müllen, J. Takeya, *Chem. Mater.* **2016**, 28, 420.
- [66] H. H. Choi, K. Cho, C. D. Frisbie, H. Sirringhaus, V. Podzorov, *Nat. Mater.* **2018**, 17, 2.
- [67] H. Yan, Z. Chen, Y. Zheng, C. Newman, J. R. Quinn, F. Dötz, M. Kastler, A. Facchetti, *Nature* **2009**, 457, 679.
- [68] A. Luzzio, L. Criante, V. D'Innocenzo, M. Caironi, *Sci. Rep.* **2013**, 3, 3425.
- [69] S. G. Bucella, A. Luzzio, E. Gann, L. Thomsen, C. R. McNeill, G. Pace, A. Perinot, Z. Chen, A. Facchetti, M. Caironi, *Nat. Commun.* **2015**, 6, 8394.
- [70] U. Zschieschang, H. Klauk, *Org. Electron.* **2015**, 25, 340.
- [71] A. Facchetti, T. J. Marks, *Mater. Matters* **2009**, 4.3, 64.
- [72] S. Müller, R. P. Baumann, T. Gessner, R. T. Weitz, *Phys. Status Solidi RRL* **2016**, 10, 339.
- [73] U. Zschieschang, K. Amsharov, M. Jansen, K. Kern, H. Klauk, R. T. Weitz, *Org. Electron.* **2015**, 26, 340.
- [74] M. Kettner, Z. Mi, D. Kalblein, J. Brill, P. W. M. Blom, R. T. Weitz, *Adv. Electron. Mater.* **2019**, 5, 1900295.
- [75] J. Rivnay, R. M. Owens, G. G. Malliaras, *Chem. Mater.* **2014**, 26, 679.
- [76] D. T. Simon, E. O. Gabrielson, K. Tybrandt, M. Berggren, *Chem. Rev.* **2016**, 116, 13009.
- [77] J. Rivnay, S. Inal, B. A. Collins, M. Sessolo, E. Stavridou, X. Strakosas, C. Tassone, D. M. Delongchamp, G. G. Malliaras, *Nat. Commun.* **2016**, 7, 11287.
- [78] M. Berggren, A. Richter-Dahlfors, *Adv. Mater.* **2007**, 19, 3201.
- [79] M. Nikolov, G. G. Malliaras, *Chem. Rec.* **2008**, 8, 13.
- [80] L. Groenendaal, F. Jonas, D. Freitag, H. Pielartzik, J. R. Reynolds, *Adv. Mater.* **2000**, 12, 481.
- [81] M. Lefebvre, Z. Qi, D. Rana, P. G. Pickup, *Chem. Mater.* **1999**, 11, 262.
- [82] A. M. Nardes, M. Kemerink, R. A. J. Janssen, J. A. M. Bastiaansen, N. M. M. Kiggen, B. M. W. Langeveld, A. J. J. M. van Breemen, M. M. de Kok, *Adv. Mater.* **2007**, 19, 1196.
- [83] A. Elschner, *PEDOT: Principles and Applications of an Intrinsically Conductive Polymer*, CRC Press, Boca Raton, FL **2011**.
- [84] C. M. Palumbiny, J. Schlipf, A. Hexemer, C. Wang, P. Müller-Buschbaum, *Adv. Electron. Mater.* **2016**, 2, 1500377.
- [85] E. Stavridou, P. Leleux, H. Rajaona, D. Khodagholy, J. Rivnay, M. Lindau, S. Sanaur, G. G. Malliaras, *Adv. Mater.* **2013**, 25, 4488.
- [86] C. Duc, A. Vlandas, G. G. Malliaras, V. Senez, *Soft Matter* **2016**, 12, 5146.
- [87] H. Shi, C. Liu, Q. Jiang, J. Xu, *Adv. Electron. Mater.* **2015**, 1, 1500017.
- [88] Y. H. Kim, C. Sachse, M. L. Machala, C. May, L. Müller-Meskamp, K. Leo, *Adv. Funct. Mater.* **2011**, 21, 1076.
- [89] T.-R. Chou, S.-H. Chen, Y.-T. Chiang, T.-T. Chang, C.-W. Lin, C.-Y. Chao, *Org. Electron.* **2017**, 48, 223.
- [90] H. S. White, G. P. Kittleson, M. S. Wrighton, *J. Am. Chem. Soc.* **1984**, 106, 5375.
- [91] J. Rivnay, P. Leleux, M. Sessolo, D. Khodagholy, T. Hervé, M. Fiocchi, G. G. Malliaras, *Adv. Mater.* **2013**, 25, 7010.
- [92] L. Q. Flagg, C. G. Bischak, J. W. Onorato, R. B. Rashid, C. K. Luscombe, D. S. Ginger, *J. Am. Chem. Soc.* **2019**, 141, 4345.
- [93] D. A. Bernards, G. G. Malliaras, *Adv. Funct. Mater.* **2007**, 17, 3538.
- [94] J. Rivnay, S. Inal, A. Salleo, R. M. Owens, M. Berggren, G. G. Malliaras, *Nat. Rev. Mater.* **2018**, 3, 17086.

- [95] A. Williamson, M. Ferro, P. Leleux, E. Ismailova, A. Kaszas, T. Doublet, P. Quilichini, J. Rivnay, B. Rózsa, G. Katona, C. Bernard, G. G. Malliaras, *Adv. Mater.* **2015**, 27, 4405.
- [96] C. Yao, Q. Li, J. Guo, F. Yan, I.-M. Hsing, *Adv. Healthcare Mater.* **2015**, 4, 528.
- [97] D. Khodagholy, T. Doublet, P. Quilichini, M. Gurfinkel, P. Leleux, A. Ghestem, E. Ismailova, T. Hervé, S. Sanaur, C. Bernard, G. G. Malliaras, *Nat. Commun.* **2013**, 4, 1575.
- [98] A. Campana, T. Cramer, D. T. Simon, M. Berggren, F. Biscarini, *Adv. Mater.* **2014**, 26, 3874.
- [99] X. Gu, C. Yao, Y. Liu, I.-M. Hsing, *Adv. Healthcare Mater.* **2016**, 5, 2345.
- [100] M. Ramuz, K. Margita, A. Hama, P. Leleux, J. Rivnay, I. Bazin, R. M. Owens, *ChemPhysChem* **2015**, 16, 1210.
- [101] J. Rivnay, P. Leleux, A. Hama, M. Ramuz, M. Huerta, G. G. Malliaras, R. M. Owens, *Sci. Rep.* **2015**, 5, 11613.
- [102] L. H. Jameson, S. A. Tria, D. Khodagholy, M. Gurfinkel, E. Lanzarini, A. Hama, G. G. Malliaras, R. M. Owens, *Adv. Mater.* **2012**, 24, 5919.
- [103] M. Chittorelli, L. V. Lingstedt, P. Romele, N. I. Crăciun, Z. Miklós Kovács-Vajna, P. W. M. Blom, F. Torricelli, *Nat. Commun.* **2018**, 9, 1441.
- [104] L. V. Lingstedt, M. Chittorelli, M. Bruckner, J. Reinholz, N. I. Crăciun, F. Torricelli, V. Mailänder, P. Gkoupidenis, P. W. M. Blom, *Adv. Healthcare Mater.* **2019**, 8, 1900128.
- [105] D. A. Bernards, D. J. Macaya, M. Nikolou, J. A. DeFranco, S. Takamatsu, G. G. Malliaras, *J. Mater. Chem.* **2008**, 18, 116.
- [106] M. Braendlein, A.-M. Pappa, M. Ferro, A. Lopresti, C. Acquaviva, E. Mamessier, G. G. Malliaras, R. M. Owens, *Adv. Mater.* **2017**, 29, 1605744.
- [107] D. Khodagholy, V. F. Curto, K. J. Fraser, M. Gurfinkel, R. Byrne, D. Diamond, G. G. Malliaras, F. Benito-Lopez, R. M. Owens, *J. Mater. Chem.* **2012**, 22, 4440.
- [108] S. Casalini, F. Leonardi, T. Cramer, F. Biscarini, *Org. Electron.* **2013**, 14, 156.
- [109] G. Scheiblin, A. Aliane, R. Coppard, R. M. Owens, P. Mailley, G. G. Malliaras, in *Fully Printed Metabolite Sensor using Organic Electrochemical Transistor*, Vol. 9568, SPIE, San Diego, CA **2015**, p. 95681E.
- [110] H. Tang, P. Lin, H. L. W. Chan, F. Yan, *Biosens. Bioelectron.* **2011**, 26, 4559.
- [111] Y. Kim, J. Do, J. Kim, S. Y. Yang, G. G. Malliaras, C. K. Ober, E. Kim, *Jpn. J. Appl. Phys.* **2010**, 49, 01AE10.
- [112] A.-M. Pappa, V. F. Curto, M. Braendlein, X. Strakosas, M. J. Donahue, M. Fiocchi, G. G. Malliaras, R. M. Owens, *Adv. Healthcare Mater.* **2016**, 5, 2295.
- [113] E. Bihar, Y. Deng, T. Miyake, M. Saadaoui, G. G. Malliaras, M. Rolandi, *Sci. Rep.* **2016**, 6, 27582.
- [114] G. Scheiblin, R. Coppard, R. M. Owens, P. Mailley, G. G. Malliaras, *Adv. Mater. Technol.* **2017**, 2, 1600141.
- [115] P. Gkoupidenis, N. Schaefer, X. Strakosas, J. A. Fairfield, G. G. Malliaras, *Appl. Phys. Lett.* **2015**, 107, 263302.
- [116] P. Gkoupidenis, N. Schaefer, B. Garlan, G. G. Malliaras, *Adv. Mater.* **2015**, 27, 7176.
- [117] Y. van de Burgt, E. Lubberman, E. J. Fuller, S. T. Keene, G. C. Faria, S. Agarwal, M. J. Marinella, A. Alec Talin, A. Salleo, *Nat. Mater.* **2017**, 16, 414.
- [118] D. A. Koutsouras, T. Prodromakis, G. G. Malliaras, P. W. M. Blom, P. Gkoupidenis, *Adv. Intell. Syst.* **2019**, 1, 1900013.